JOURNAL OF MATERIALS SCIENCE 27 (1992) 6204–6212

Microstructure and microanalysis of hardened cement pastes involving ground granulated blast-furnace slag

I. G. RICHARDSON, G. W. GROVES
Department of Materials, Oxford University, Oxford OX1 3PH, UK

The microstructure and composition of hardened cement pastes of a wide range of blends of ground granulated blast-furnace slag with ordinary Portland cement have been studied, using techniques of transmission electron microscopy with microanalysis combined with electron microprobe analysis. Throughout the range, a calcium silicate hydrate gel (C–S–H) is the dominant cementing phase, present in the "inner product" within the space originally occupied by either slag grains or alite or belite grains originating from the Portland cement, or in the "outer product" in the originally water-filled spaces. The morphology and composition of the outer product C–S–H and the composition of inner product C–S–H change with blend composition. Inner product of slag grains contains C–S–H of the same composition as the outer product C–S–H, intimately mixed with a Mg, Al-rich hydroxide phase whose fineness shows considerable variation. Inner product C–S–H of alite or belite does not differ significantly in Ca : Si ratio from that of slag. The reduction of Ca : Si ratio of all forms of C–S–H with increasing slag loading may have implications for the pH-buffering capacity of blends of large slag loading.

1. Introduction

Molten slag produced during the manufacture of pig-iron if cooled sufficiently rapidly forms a glassy material having latent hydraulic properties. When ground to a fineness similar to that of ordinary Portland cement (OPC) it does react with water to produce hydrates, but the reaction is so slow that for practical purposes it needs to be activated, most commonly by blending the slag with OPC. The partial replacement of OPC with ground granulated blast-furnace slag (GGBFS) has reported benefits, including lower chloride diffusion rates at 25 °C [1], and a greater resistance to sulphate attack [2]. The hydraulicity of the slag is affected by various factors, including the composition, which can vary widely, the glass content, and the particle size distribution. Taylor [3] has recently reviewed the extensive literature on cements containing GGBFS.

Although much is known of the hydration chemistry of slag cements [3], there is relatively little knowledge of the microstructure of hardened pastes at the level of resolution which can be achieved using techniques of transmission electron microscopy (TEM) with associated high-resolution microanalysis. This paper presents the results of applying this technique to the study of GGBFS/OPC blends (slag fraction 0–1), combined with electron microprobe analysis (EMPA).

2. Experimental procedure

Single batches of a Blue Circle (Northfleet) OPC and a Frodingham Cement Co. CEMSAVE GGBFS, were used. The oxide composition of these cements is shown in Table I. Pastes were prepared by mixing the required amounts of solids with de-ionized water at a liquid to solids ratio of 0.4. The resulting paste was placed in a plastic tube which was then sealed in a plastic bag before placing in a curing bath, generally set at 20 °C. For X-ray diffraction and thermal analysis, samples were crushed and washed in propan-2-ol before storing in a vacuum desiccator prior to analysis. The experimental techniques are described in a previous paper [6], as is the preparation of specimens for TEM and EMPA.

3. Results and discussion

3.1. Hydration products

Heat evolution curves for blends typically have a double peak as shown in Fig. 1 for a 1 : 1 GGBFS/OPC paste. Following the development of the hydration phases by thermal analysis reveals that the second peak is unlikely to correspond to the formation of an AFm phase, as has been suggested previously [7, 8], but more probably to the formation of secondary AFt; the development of long needles of AFt during this heat peak has previously been confirmed by scanning electron microscope studies [9]. It is interesting to note that the production of $Ca(OH)_2$ is initially in excess of that which is expected from the OPC content alone, indicating an accelerating effect of the GGBFS on OPC hydration although a dip in $Ca(OH)_2$ production corresponds to the initial reaction of the GGBFS. As has been previously reported [10], the $Ca(OH)_2$ content eventually (after about

0022–2461

TABLE I Oxide compositions (wt %) supplied with the Blue Circle Northfleet OPC and Frodingham Cement Co. CEMSAVE GGBFS

Oxide	OPC	GGBFS
Na_2O	0.19	0.64
MgO	1.33	7.74
Al_2O_3	6.19	11.00
SiO_2	20.00	37.20
SO_3[a]	2.65	3.68
K_2O	0.86	0.55
CaO	65.90	41.70
TiO_2	0.30	0.68
Mn_2O_3[b]	0.06	0.73
Fe_2O_3[b]	3.03	0.38

[a] Most sulphur in GGBFS is present in its lowest oxidation state (as S^{2-}) [4, 5].

[b] Manganese and iron are present in the glassy slag in lower oxidation states [3]. Some colloidal and free iron are likely to be present in the GGBFS [5].

100 h) falls below that expected from the OPC content due to pozzolanic reaction. In a 1:1 blend the amount of $Ca(OH)_2$ present remains substantial for times in excess of 10^4 h, but in the long term very low $Ca(OH)_2$ contents can be expected in blends with GGBFS/OPC proportions in excess of 3:1.

Although the formation of AFm phases continues after the termination of the main heat peak, X-ray diffraction traces show that the AFt phase persists in 1:1 blends for at least 2 months. Thermal analysis shows that the AFm content reaches a maximum after roughly 10^3 h and then diminishes slowly with time, for blends of 1:1, 3:1 and 9:1 GGBFS/OPC. This decrease is possibly accompanied by an increase in AFt (the development of a shoulder on the C–S–H decomposition peak of the DSC curve is consistent with this), which may be connected with the slow release of S^{2-} species as the slag reacts. However, the behaviour of the S^{2-} ion present in the slag is not well understood [5].

On the X-ray diffraction traces there also appear peaks which are believed to correspond to a Mg, Al-rich phase similar to the naturally occurring mineral hydrotalcite. Typically, this phase was first detected in the slag blends after 2–4 days.

3.2. Microstructures

Microstructural features can be broadly classified into outer product, formed in the originally water-filled

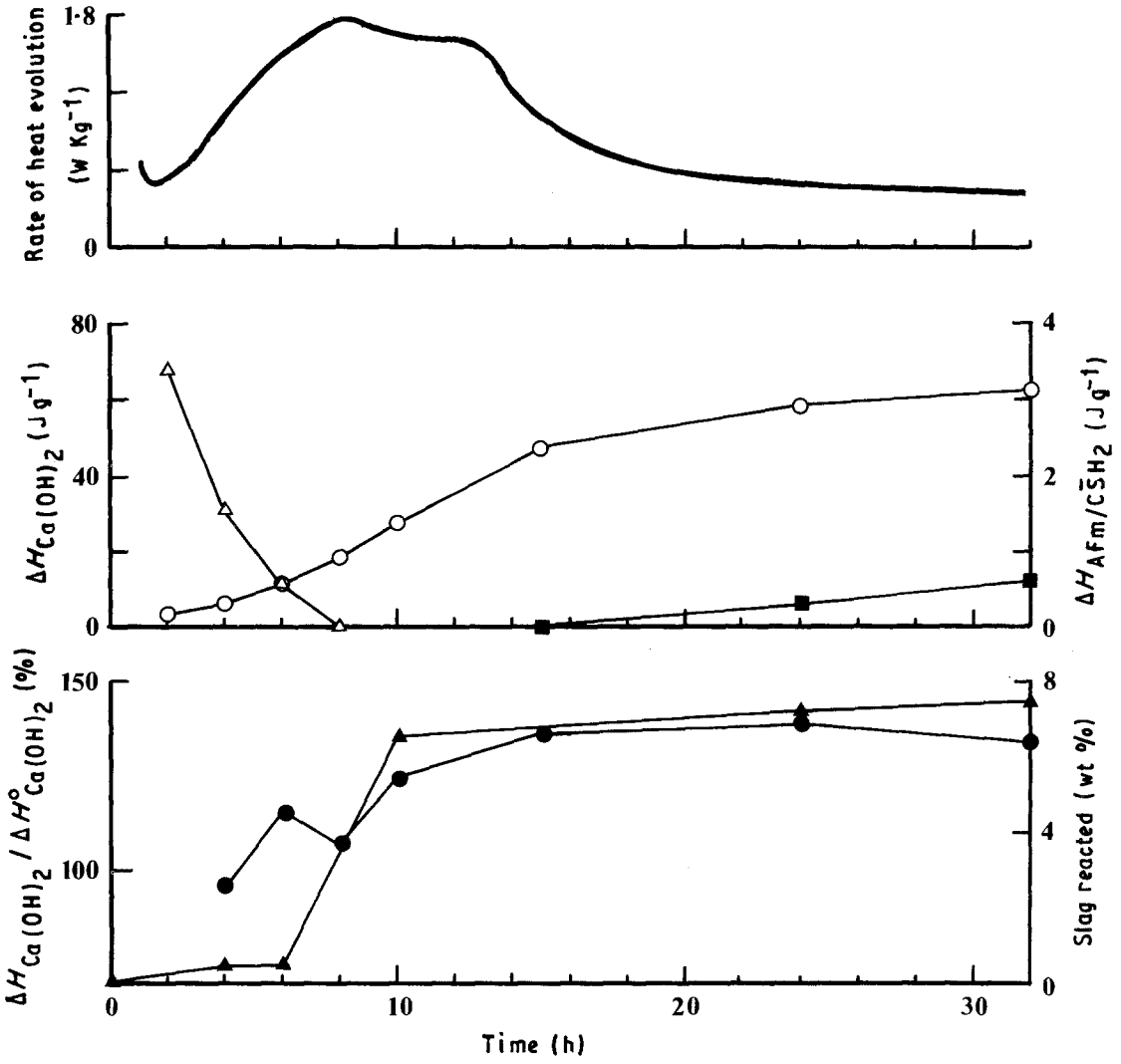

Figure 1 (a) Rate of heat evolution curve for a 1:1 GGBFS/OPC blend (W/S = 0.4, 20 °C) and (b, c) the corresponding production of (○) $Ca(OH)_2$ and (■) AFm, the consumption of (△) gypsum and (▲) slag, and (●) the ratio of $Ca(OH)_2$ content to that expected from the dilution of OPC in the blend.

spaces, and inner product, formed within the boundaries of the original anhydrous grains.

3.2.1. Outer product (Op)

The major phases present in the outer product region of neat OPC pastes are C–S–H gel, $Ca(OH)_2$, AFm and AFt. The introduction of GGBFS into this system alters the quantity of these phases, the composition of the AFm and in the case of C–S–H gel, the composition and morphology. The morphology of Op C–S–H is affected by the slag loading. In pure OPC or in low slag blends, the C–S–H has a strongly linear directional characteristic, being fibrillar in its appearance in the TEM. At ~ 75% GGBFS regions of foil-like C–S–H form without these linear characteristics. As the slag fraction is increased, the foil-like morphology gradually replaces the fibrillar morphology. Fig. 2 shows both the fine fibrillar and foil-like C–S–H in a 75% slag blend, and Fig. 3 shows an area in a 90% blend which is totally foil-like in morphology. C–S–H exhibiting the fibrillar morphology occurs in all blends except the neat GGBFS system. The foil-like morphology may be coarser or finer, probably depending on space constraints upon the growth of the C–S–H; Fig. 3 shows an example of a relatively fine morphology. Although the linear, fibrillar morphology has only fine porosity, its inefficient filling of space appears to leave some fairly coarse, interconnected pores, whilst the more evenly distributed pores of the foil-like C–S–H are probably less well interconnected. This may account for the beneficial effects of slag in reducing diffusion rates in blended pastes [1].

The aluminate hydrates AFt and AFm can occur in all the OPC-bearing blends. These phases are found to be identical in morphology to those present in neat OPC pastes. An example of small AFm plates can be seen in the upper central part of Fig. 2. It is notable how the AFm merges with the outer product C–S–H. AFt is largely dehydrated by conditions of specimen preparation for the TEM but relicts are visible, as in Fig. 4, where the identification as AFt is by microanalysis of the relicts. Needle-like AFt crystals corresponding to the relicts seen in TEM are, of course, readily identified in scanning electron microscope observations of fracture surfaces [9].

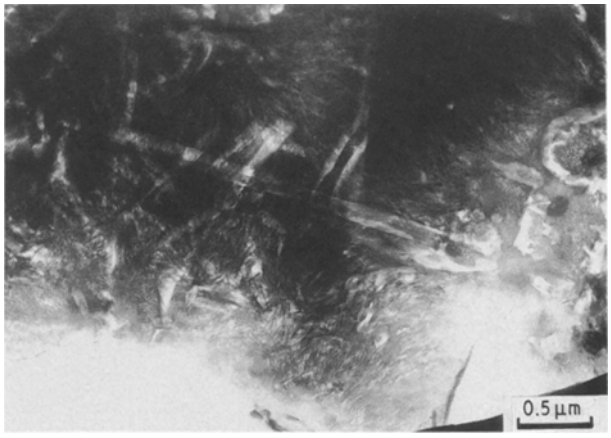

Figure 2 Transmission electron micrograph showing both fine-fibrillar and foil-like Op, C–S–H in a 75% slag blend (W/S = 0.4, 20 °C, 14 months).

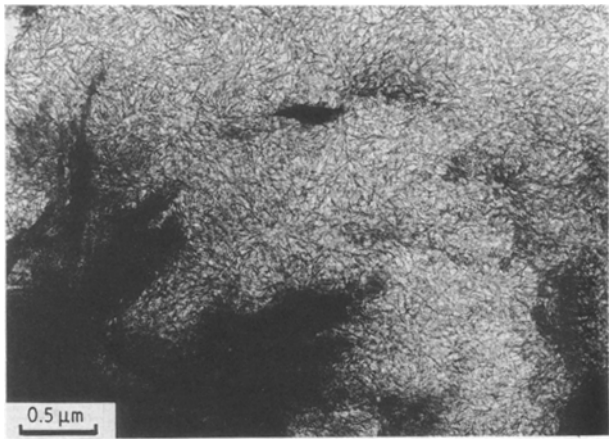

Figure 3 Transmission electron micrograph showing foil-like Op C–S–H in a 90% slag blend (W/S = 0.4, 20 °C, 14 months).

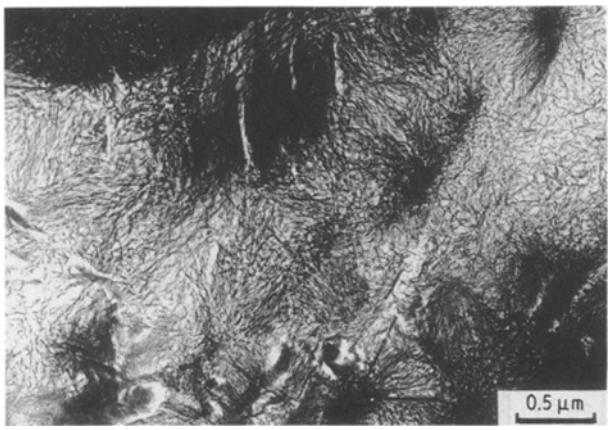

Figure 4 Transmission electron micrograph showing AFt relicts in the outer product region of a 10% slag blend (W/S = 0.4, 20 °C; 14 months).

3.2.2. Inner product (Ip)

Inner product regions derived from hydrating alite or belite grains within blends are morphologically identical to those occurring in neat OPC pastes. In mature pastes, fully hydrated small grains of both alite and GGBFS often display a coarse morphology. Fig. 5 shows inner product regions derived from small grains of both alite and slag in a 1:1 blend. As with alite grains, larger slag grains most often have a rim of fine textured C–S–H which can persist for many years and which merges into Op C–S–H as shown in Fig. 6. Frequently Mg, Al-rich laths or possibly platelets are seen within the Ip C–S–H. These may be oriented to run towards the outer boundary of the Ip C–S–H as previously reported [11], but in other cases they are randomly oriented even at the outer boundary. Fig. 7 illustrates the former case, whilst an example of randomly oriented laths is shown in Fig. 8, which also shows, at the Ip/Op interface, plates of AFm and relicts of AFt needles sectioned approximately normal to the length of the needles. The composition of the

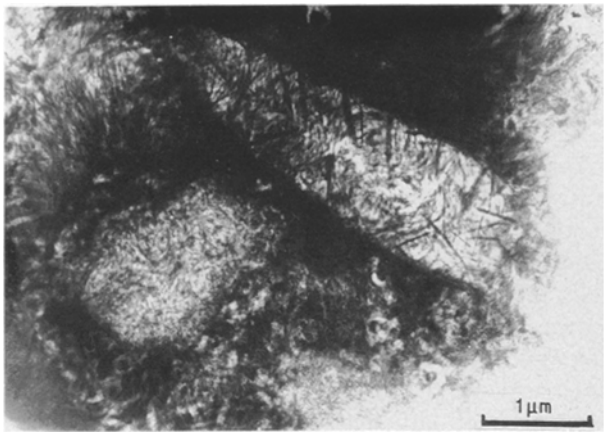

Figure 5 Transmission electron micrograph showing small, fully reacted alite and slag (top) grains with coarse Ip C–S–H in a 50% slag blend (W/S = 0.4, 20 °C, 12 months).

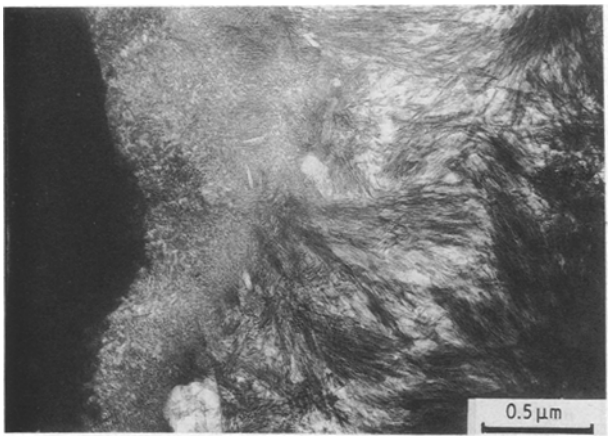

Figure 6 Transmission electron micrograph showing unreacted slag (left), fine-textured Ip C–S–H (centre-left) and finefibrillar Op, C–S–H in a 67% slag blend (W/S = 0.4, 20 °C, 14 months).

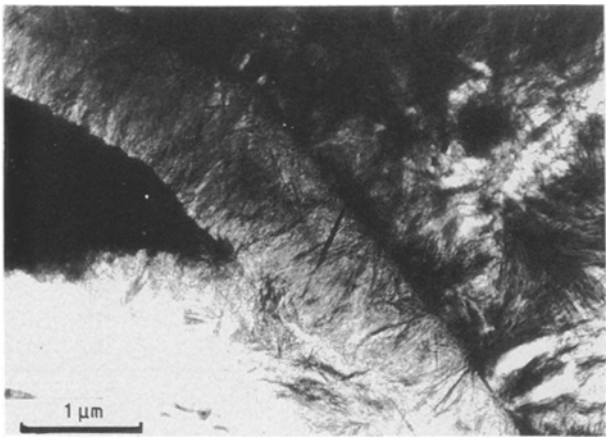

Figure 7 Transmission electron micrograph showing a well-defined slag inner product region containing C–S–H and Mg, Al-rich precipitates which are oriented towards the Ip/Op interface.

precipitates within the Ip is discussed later. They have been previously identified as plates from scanning electron microscope (SEM) observation in a TEM and SEM study [11, 12], and this has been confirmed for small grains in this work. However, even for small

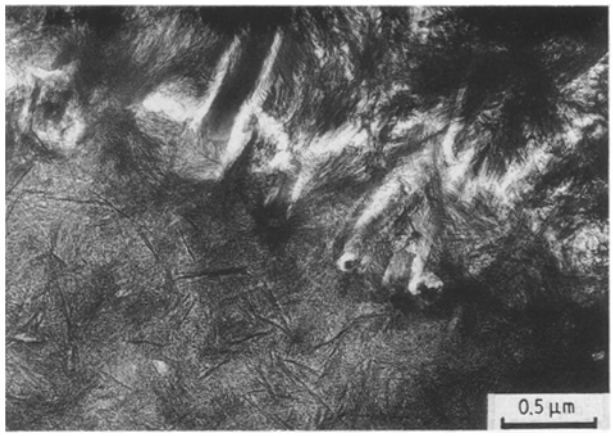

Figure 8 Transmission electron micrograph showing Mg, Al-rich precipitates randomly distributed within a slag inner product region (lower left-centre), fine fibrillar Op C–S–H (upper right-centre), an AFm plate (upper left-centre) and several AFt relicts along the Ip/Op interface (50% slag blend, W/S = 0.4, 20 °C, 3 months).

grains, the SEM can give a misleading impression of the general proportion of the quantity of plates to that of C–S–H gel, and this seems to have led Feng and Glasser [12] to the doubtful conclusion that C–S–H is present in only minor amounts within the inner slag hydrate of mature pastes; certainly their assertion is not true for the systems studied here. When the plates are very well developed, as for example in Fig. 9, they may indeed predominate over the C–S–H gel but in many other inner product regions, even in 3 year old pastes, the plates are less well developed and a high proportion of C–S–H gel is present, as in Fig. 8. The development of the plates occurs to different extents in different slag grains, possibly depending on composition and also appearing to depend on particle size, because platelets or laths typically appear very early in small grains. Although in the later stages of development the precipitates are undoubtedly plates, as previously reported [11, 12], in the early stages it is not obvious from the observations that the morphology is plate-like, and they are probably better described as laths or needles. Various stages of microstructural evolution of the precipitates can be seen simultaneously within the same specimen.

The final microstructural feature to be noted is the presence of small, almost round, poorly crystalline particles as seen on the right-hand side of Fig. 9. The particles are rich in iron and aluminium and also often contain significant amounts of titanium. They appear similar to particles reported to occur in OPC and PFA/OPC pastes [13] where they were considered to be a poorly crystalline form of a calcium-deficient hydrogarnet.

3.3. Microanalysis

Tables II and III give the results of an extensive set of analyses of inner and outer product C–S–H obtained in the TEM for 1 : 1 GGBFS/OPC blended paste. The Ca : Si ratios of the C–S–H gels are seen to be consistently lower than those of gels in hardened OPC pastes, where a typical average value for the Ca : Si ratio is 1.8

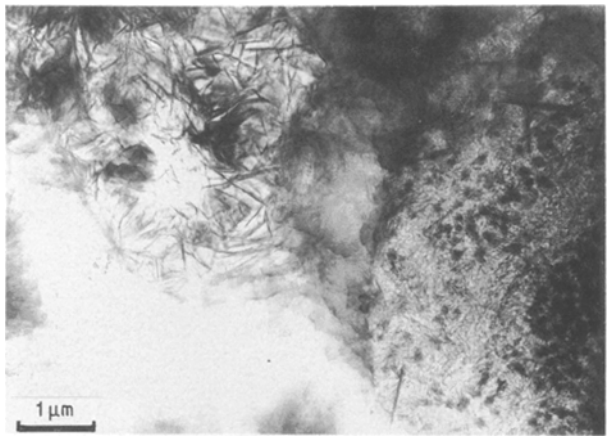

Figure 9 Transmission electron micrograph showing very well-developed Mg, Al-rich laths (upper left) and small round Fe, Al-rich particles (right) in a 75% slag blend (W/S = 0.4, 50 °C, 2 years).

[6]. It is further seen that there is no significant difference between the Ca:Si ratio of C–S–H gels in the inner product of alite, the inner product of slag and the outer product, nor is there any significant change in Ca:Si ratio with the curing time of the paste. It should be emphasized that these statements apply to averages and that there is considerable local variation in gel composition. This variation is confirmed by EMPA analysis of 1:1 blends where, for example, two distant gel areas in the same specimen gave significantly different Ca:Si ratios of 1.2 and 1.45, or in another example where regions of gel in pastes of two different ages gave values of 1.7 and 1.43. These different values were derived from large numbers of determinations in the same local area (less than 60 μm × 60 μm). This shows that results obtained from localized data sets, even if these are large sets, cannot be taken to establish compositional averages and trends. This may help to explain the apparent discrepancy between the results of Table II and those of Harrisson *et al.* [14]. who gave a Ca:Si ratio of a C–S–H in a 40% slag blend only marginally lower than C–S–H in neat OPC pastes.

Table III shows that although the Ca:Si ratios of inner product gels of alite (or belite) and slag do not, on average, differ significantly, there is a marked difference in the aluminium content which is substantially greater in the slag inner product. This is also shown in EMPA analysis, for example Fig. 10, where slag and slag inner product regions are seen to have similar (Al + Fe):Ca ratios, higher than those of OPC inner product, although the slag itself has a higher Si:Ca ratio than its inner product. The best chemical marker for slag inner product is the magnesium content. As reported previously [14], magnesium does not migrate from the volume originally occupied by the slag grain and the loss of other elements, particularly silicon, from the volume which becomes occupied by inner product C–S–H causes the slag inner product C–S–H to show the highest magnesium concentration in the microstructure. It is thus revealed clearly on EMPA magnesium maps, for example Fig. 11. TEM microanalysis confirms that magnesium is never found in outer product C–S–H. Transmission electron micrographs of slag inner product presented earlier show that precipitates which eventually become platelike develop in the slag inner product. Even with the relatively high resolution of microanalysis in the TEM, the precipitates are generally so small that analysed areas contain both gel and precipitate and this is even more the case for the much larger volumes analysed in EMPA. The combination of Mg:Ca and Al:Ca analyses by TEM and EMPA. for slag inner product in a 1:1 GGBFS/OPC blend is shown in Fig. 12. Remarkable agreement between the two techniques is shown. In some analyses in the TEM, the

TABLE II Ca:Si atom ratios in hardened GGBFS/OPC 1:1 pastes. W/S = 0.4, 20 °C

Age	Mean ± $\sigma_{n-1}(n)$		
	Ip C–S–H^{BFS}	Ip C–S–H^{OPC}	Op C–S–H
1 week	1.63 ± 0.14 (14)	1.59 ± 0.18 (17)	1.52 ± 0.14 (26)
4 weeks	1.52 ± 0.15 (12)	1.44 ± 0.06 (10)	1.42 ± 0.10 (23)
3 months	1.47 ± 0.16 (17)	1.38 ± 0.12 (3)	1.40 ± 0.08 (25)
1 year 1	1.56 ± 0.10 (12)	1.56 ± 0.13 (7)	1.57 ± 0.09 (19)
1 year 2	1.54 ± 0.12 (11)	1.43 ± 0.16 (3)	1.52 ± 0.15 (16)
3 years	1.54 ± 0.13 (9)	1.47 ± 0.09 (10)	1.51 ± 0.07 (6)

TABLE III Al:Ca atom ratios in hardened GGBFS/OPC 1:1 pastes. W/S = 0.4, 20 °C

Age	Mean ± $\sigma_{n-1}(n)$		
	Ip C–S–H^{BFS}	Ip C–S–H^{OPC}	Op C–S–H
1 week	0.21 ± 0.07 (14)	0.10 ± 0.01 (6)	0.10 ± 0.01 (9)
4 weeks	0.32 ± 0.13 (12)	0.11 ± 0.01 (5)	0.11 ± 0.01 (14)
3 months	0.33 ± 0.11 (16)	0.11 ± 0.02 (2)	0.11 ± 0.01 (17)
1 year 1	0.32 ± 0.14 (13)	–	0.12 ± 0.02 (6)
1 year 2	0.28 ± 0.08 (13)	0.10 ± 0.01 (4)	0.09 ± 0.01 (12)
3 years	0.32 ± 0.14 (7)	0.11 ± 0.01 (7)	0.12 ± 0.01 (6)

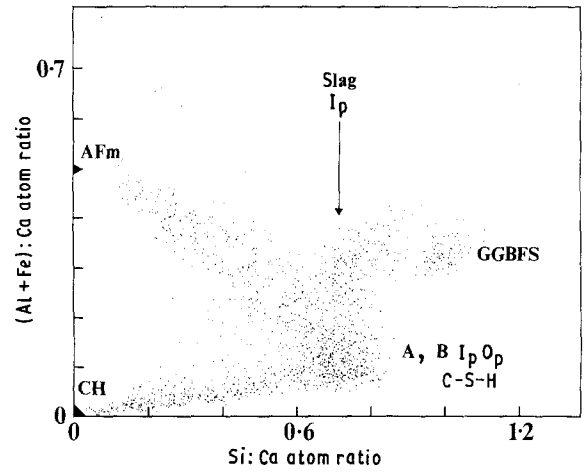

Figure 10 (Al + Fe):Ca against Si:Ca atom ratio plot for a 25% slag blend (EMPA mapping data for area in Fig. 11). A, B Ip = alite and belite inner product.

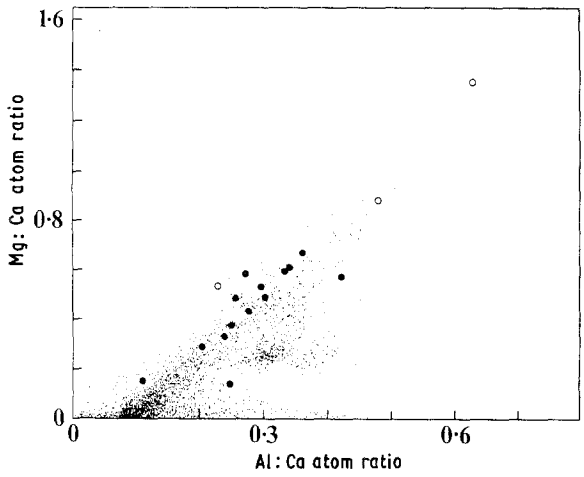

Figure 12 Mg:Ca against Al:Ca atom ratio plot of the EMPA mapping data of an area in a 50% slag blend, and TEM analyses of (●) fine homogeneous inner product and (○) mixtures of this with Mg, Al-rich laths (W/S = 0.4, 20 °C, 14 months).

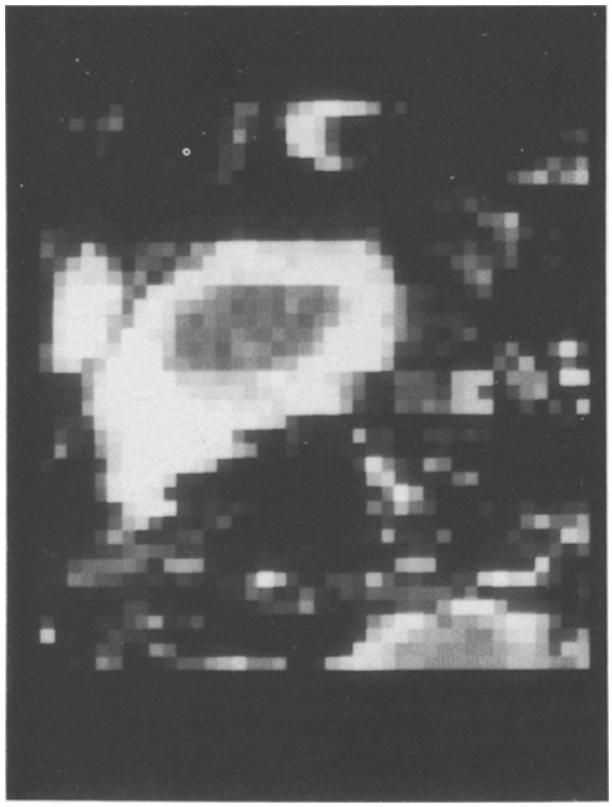

Figure 11 Magnesium map for an area in a 25% slag blend (W/S = 0.4, 20 °C, 14 months) (one square = 1 μm^2).

precipitates could be seen within the analysis volume, whereas in EMPA the precipitates are, of course, never observable. Nevertheless, all the data fall quite well on a single straight trend line which can be described by the equation

$$\text{Al:Ca} = x + 0.41(\text{Mg:Ca}) \quad (1)$$

where $0.045 < x < 0.141$. The Al:Ca ratios of the outer product and OPC inner product gel fall within the range of values possible for x in Equation 1. It therefore seems reasonable to consider x as the Al:Ca ratio of single-phase C–S–H within the 1:1 slag/OPC system. The slag inner product can therefore be envisaged as an intimate mixture of this single-phase C–S–H, compositionally identical to outer product C–S–H, and a Mg, Al-rich hydroxide phase with, in this case, a Mg:Al atom ratio of 2.4. A similar assumption was made by Harrisson *et al.* [14] although they considered the C–S–H in slag inner product to have a lower Ca:Si ratio than that in hydrated alite or belite grains, which is not borne out by our results. The fact that TEM analyses of slag inner product in which plate- or lath-like precipitates were not clearly recognizable are consistent with this approach, suggest that the phase mixture can occur on a very fine scale. The observable precipitation of Mg, Al-rich laths, or eventually distinct plates with ageing, can be considered as a coarsening of this very fine phase mixture.

Slag inner product regions are also rich in titanium, manganese and iron and EMPA element maps of titanium, in particular, are effective in showing the regions of slag inner product in the same way as magnesium maps. The relatively low concentration of these elements requires the maps to be collected by wavelength dispersive detectors.

The effect of slag loading on compositional trends was also investigated. Tables IV and V show the results of an extensive series of TEM microanalyses. The inner product C–S–H from alite and belite grains is represented in Tables IV and V by the Ip C–S–H^{OPC} column. It is evident that the chemical composition of these regions essentially mirrors that of the Op C–S–H in all the blends, although this fact should not be taken to show that they are structurally identical; for example, the inner product C–S–H could be more highly polymerized, as suggested by MacPhee *et al.* [15]. All the C–S–H gels show a similar trend of reducing Ca:Si ratio with increase in slag loading. The results are shown graphically for outer product C–S–H in Fig. 13. The trend for C–S–H gels of inner product regions is closely similar. The results have an important implication for the buffering capacity of the pastes of large slag loadings, in which the long-term

TABLE IV Ca:Si atom ratios in hardened GGBFS/OPC blends. W/S = 0.4, 20 °C, 14 months

% GGBFS	Mean ± σ_{n-1} (n)		
	Ip C–S–H^{BFS}	Ip C–S–H^{OPC}	Op C–S–H
0[a]	–	1.80 ± 0.15 (107)	1.70 ± 0.12 (85)
10	1.90 ± 0.12 (21)	1.90 ± 0.10 (13)	1.86 ± 0.11 (14)
25	1.80 ± 0.17 (15)	1.75 ± 0.14 (14)	1.79 ± 0.15 (24)
50[a]	1.55 ± 0.11 (23)	1.52 ± 0.13 (10)	1.55 ± 0.12 (35)
66.7	1.48 ± 0.07 (22)	1.32 ± 0.10 (2)	1.42 ± 0.08 (27)
75	1.40 ± 0.12 (12)	1.41 ± 0.13 (3)	1.34 ± 0.07 (21)
83.3	1.43 ± 0.08 (21)	1.21 ± 0 (1)	1.34 ± 0.06 (22)
90[a]	1.26 ± 0.10 (39)	1.29 ± 0.09 (6)	1.29 ± 0.07 (85)
100	1.09 ± 0.08 (25)	–	1.18 ± 0.06 (26)

[a] More than one specimen.

TABLE V Al:Ca atom ratios in hardened GGBFS/OPC blends W/S = 0.4, 20 °C, 14 months

% GGBFS	Mean ± σ_{n-1} (n)		
	Ip C–S–H^{BFS}	Ip C–S–H^{OPC}	Op C–S–H
0[a]	–	0.09 ± 0.03 (10)	0.09 ± 0.01 (10)
10	0.23 ± 0.05 (20)	0.09 ± 0.04 (2)	0.09 ± 0 (2)
25	0.25 ± 0.10 (15)	0.08 ± 0.01 (7)	0.09 ± 0.02 (18)
50[a]	0.30 ± 0.11 (23)	0.10 ± 0.01 (4)	0.10 ± 0.01 (18)
66.7	0.28 ± 0.07 (22)	0.14 ± 0.01 (2)	0.12 ± 0.01 (26)
75	0.30 ± 0.16 (12)	0.13 ± 0.02 (3)	0.13 ± 0.01 (21)
83.3	0.34 ± 0.11 (21)	0.17 ± 0 (1)	0.14 ± 0.02 (22)
90[a]	0.40 ± 0.17 (39)	0.15 ± 0.01 (6)	0.16 ± 0.02 (85)
100	0.41 ± 0.19 (25)	–	0.19 ± 0.06 (26)

[a] More than one specimen.

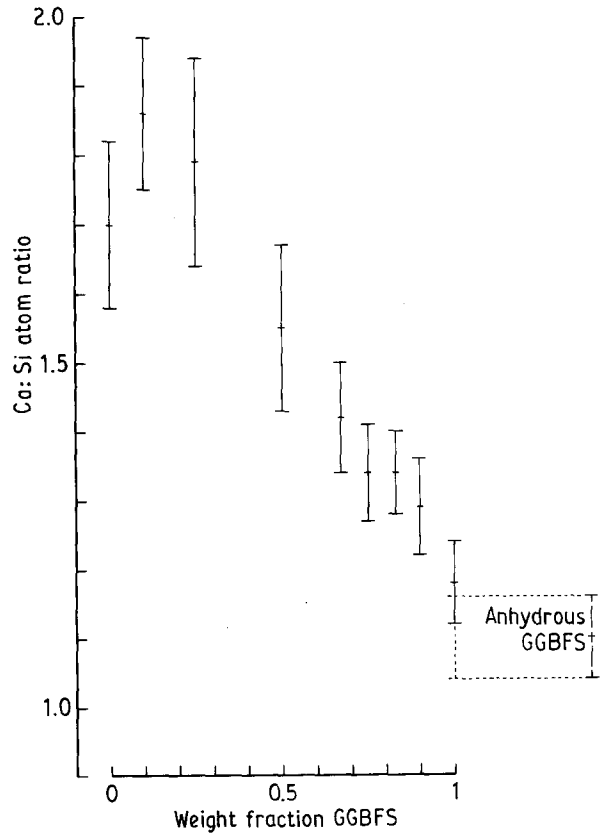

Figure 13 Variation of Ca:Si atom ratio with GGBFS loading for outer product C–S–H.

$Ca(OH)_2$ content may be low or zero. The pH level set by the C–S–H will be the lower, the lower is the Ca:Si ratio of the gel, and this may have implications for the corrosion of steel in the paste.

Table V shows that as the Ca:Si ratio of the gels decreases (Si:Ca increases), the Al:Ca ratio increases. The trend for outer product C–S–H is shown in Fig. 14 on which all the unprocessed TEM analyses for the 14 month old OPC-containing blends are plotted. This result has implications for models of the structure of C–S–H containing trivalent cations (Al^{3+} or Fe^{3+}) which will be discussed elsewhere [16].

In slag inner product, Mg:Ca ratios were measured and related to Al:Ca ratios by both TEM microanalysis and EMPA for the range of slag loadings. For all the blends, excellent agreement was obtained between the two techniques and trend lines were established. The combination of TEM and EMPA data for the 1:3 GGBFS/OPC blend is shown in Fig. 15, for example. Equations of the form

$$\text{Al:Ca} = a + b(\text{Mg:Ca}) \quad (2)$$

were fitted to the trend lines for the different blends and the result is shown in Table VI. In Equation 2 and Table VI, a is the Al:Ca ratio of the underlying single-phase C–S–H gel and b is the Al:Mg ratio of the Mg, Al hydroxide phase intermixed with the C–S–H in the slag inner product. Although the values

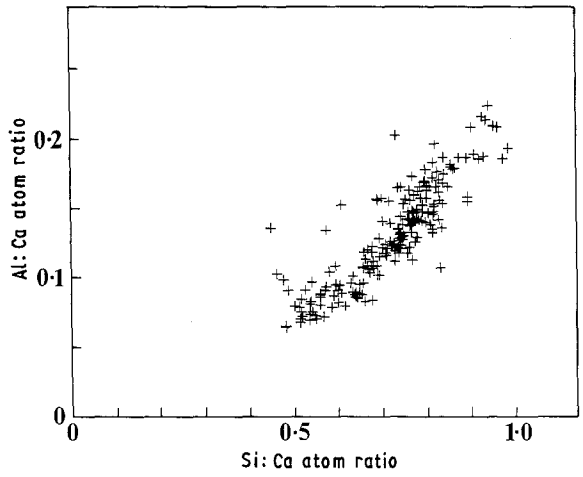

Figure 14 Al : Ca against Si : Ca atom ratio plot of the TEM data for the 14 month old OPC-containing blends.

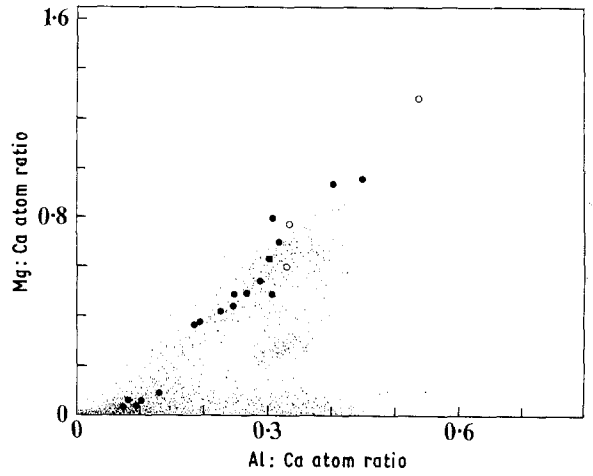

Figure 15 Mg : Ca against Al : Ca atom ratio plot of the EMPA mapping data of an area in a 25% slag blend (see Fig. 11), and TEM analyses of (●) fine homogeneous inner product and (○) mixtures of this with Mg, Al-rich laths (W/S = 0.4, 20 °C, 14 months).

TABLE VI Al : Ca = $a + b$(Mg : Ca)

% GGBFS	Al : Ca Op C–S–H	a	b	Mg : Al
0	0.052	0.042	0.373	2.68
10	–	0.04	0.402	2.49
25	–	0.064	0.434	2.30
50	0.101	0.098	0.411	2.43
66.7	0.123	0.100	0.401	2.49
75	0.133	0.121	0.418	2.39
83.3	0.140	0.132	0.420	2.38
90	0.155	0.138	0.476	2.10
100	0.194	0.185	0.568	1.76

of a are always lower than the Al : Ca ratio of outer product C–S–H, the differences are generally small and within experimental error. This observation simplifies modelling of the system over the whole range of slag loading by enabling the slag inner product to be always considered to be an intimate mixture of single-phase C–S–H, of the same or nearly the same composition as Op C–S–H, with a Mg, Al-rich phase.

TABLE VII Range of composition for AFm-type phases in GGBFS/OPS blends: $C_3(A_{1-x}F_x)\cdot C(S_yH_{1-y})\cdot H_z$

% GGBFS	y minimum	y maximum	x maximum
0	0	0.08	0.36
0[TEM]	0	0.15	0.31
10	0	0.24	0.2
25	0	0.24	0.3
50[a]	0	0.44	< 0.04
50[a]	0.2	0.60	0.4
66.7	0.24	1.00	0.22
75	0.44	1.00	0.4
83.3	0.72	1.00	0.2
90	–	–	–
100	–	–	–

[a] Two areas on same specimen.

AFm phases are found in all the OPC-bearing pastes, but not in the neat GGBFS system. Compositional ranges for these phases have been derived from EMPA mapping data, and are presented in Table VII. The results of Table VII were obtained from EMPA data similar to those shown in Fig. 10 but with plots of Fe : Ca against Al : Ca to determine values of x, and (Al + Fe) : Ca against S : Ca to determine values of y. Because of the wide scattering of points on these maps, the results are reported in terms of limit values rather than giving mean values. Despite the wide ranges a definite trend of increasing S content with increasing slag loading can be seen. The maximum y values show a quite sharp increase as the slag loading passes through 50%, consistent with a gap in the solubility of C_4ASH_{12} and C_4AH_x as reported by Taylor [17]. There is no clear trend in the level of iron substitution for aluminium.

4. Conclusion

The main phases present in hardened pastes of GGBFS/OPC cement blends are C–S–H gel, $Ca(OH)_2$, the sulpho-aluminate hydrate phases AFt and AFm and a Mg, Al-rich hydroxide phase. TEM also reveals the presence of a poorly crystalline Fe, Al-rich phase, possibly a forerunner of hydrogarnet. Although in the short term $Ca(OH)_2$ production is accelerated by the presence of GGBFS, in the long term the $Ca(OH)_2$ content is reduced by pozzolanic reaction. Microstructurally the hydration products of the blended pastes can, as in OPC pastes, be divided into inner and outer products. The inner product of slag grains is readily distinguished on EMPA maps by a higher concentration of magnesium or titanium. TEM and EMPA microanalysis of slag inner product are in good agreement and indicate an intimate mixture of C–S–H of the same composition as outer product C–S–H and a Mg, Al-rich hydroxide phase of Mg : Al atom ratio of ~ 2.4. TEM observations show that this phase varies in scale from barely resolvable linear features to clear platelets, and compositional analyses imply its presence on a scale below that resolved by TEM. The effect of increasing slag loading on outer product C–S–H is to reduce the Ca : Si ratio, increase the Al : Ca ratio and progressively change the

morphology from a strongly linear, fibrillar morphology at low-level slag loadings to a fine foil-like morphology at higher slag loadings. This latter morphology appears to fill space with a more finely distributed porosity which may help to account for the reduced diffusion rates found in pastes of slag blends. The reduction in Ca:Si ratio with increasing slag loading is similar for inner and outer product C–S–H and it implies that the C–S–H present at high slag loadings will buffer the pH of pore solutions to a lower value. AFm phases were found in all OPC-bearing pastes, though not in a neat GGBFS paste. The sulphur content of the AFm increased with increasing slag loading.

Acknowledgements

Thanks are due to SERC for financial support (IGR) and to C. R. Wilding, Harwell Laboratory, for the supply of material and helpful discussions.

References

1. C. L. PAGE, N. R. SHORT and A. EL TARRAS, *Cem. Conc. Res.* **11** (1981) 395.
2. M. REGOURD, in "Proceedings of the 7th International Congress on the Chemistry of Cement", Vol. 1 (Editions Septima, Paris, 1980) p. III-2/10.
3. H. F. W. TAYLOR, in "Cement chemistry" (Academic Press, London, 1990) p. 276.
4. H. G. SMOLCZYK, in "Proceedings of the 7th International Congress on the Chemistry of Cement", Vol. 1 (Editions Septima, Paris, 1980) p. III-1/3.
5. F. P. GLASSER, S. DIAMOND and D. M. ROY, *Mater. Res. Soc. Symp. Proc.* **85**, edited by L. J. Struble and P. W. Brown (1987) 167.
6. I. G. RICHARDSON and G. W. GROVES, *J. Mater. Sci.* **27** (1992) in press.
7. J. SKALNY, I. JAWED and H. F. W. TAYLOR, *World Cem. Technol.* **9** (1978) 183.
8. J. BENSTED, *Adv. Cem. Res.* **1** (1987) 35.
9. I. G. RICHARDSON, C. R. WILDING and M. J. DICKSON, *ibid.* **2** (1989) 147.
10. I. G. RICHARDSON, S. A. RODGER and G. W. GROVES, *Mater. Res. Soc. Symp. Proc.* **176** (1990) 63.
11. Q. L. FENG, E. E. LACHOWSKI and F. P. GLASSER, *ibid.* **137** (1989) 419.
12. Q. L. FENG and F. P. GLASSER, *ibid.* **178** (1990) 57.
13. S. A. RODGER and G. W. GROVES, *J. Amer. Ceram. Soc.* **72** (1989) 1037.
14. A. M. HARRISSON, N. B. WINTER and H. F. W. TAYLOR, *Mater. Res. Soc. Symp. Proc.* **86** (1987) 199.
15. D. E. MACPHEE, E. E. LACHOWSKI and F. P. GLASSER, *Adv. Cem. Res.* **1** (1988) 131.
16. I. G. RICHARDSON and G. W. GROVES, *Cem. Conc. Res.* (1992) to be published.
17. H. F. W. TAYLOR, in "Proceedings of the 8th International Congress on the Chemistry of Cement", Vol. 1 (FINEP, Rio de Janeiro, 1986) p. 82.

Received 15 October 1991
and accepted 29 January 1992